Dislocation networks in ^{4}He crystals

A. D. Fefferman,[1] F. Souris,[1] A. Haziot,[1] J. R. Beamish,[1,2] and S. Balibar[1]

[1]*Laboratoire de Physique Statistique de l'ENS, associé au CNRS et aux Universités D. Diderot et P.M. Curie, 24 rue Lhomond, 75231 Paris Cedex 05, France*

[2]*Department of Physics, University of Alberta, Edmonton, Alberta, Canada T6G 2E1*

(Received 10 October 2013; revised manuscript received 19 November 2013; published 16 January 2014)

The mechanical behavior of crystals is dominated by dislocation networks, their structure, and their interactions with impurities or thermal phonons. However, in classical crystals, networks are usually random with impurities often forming nonequilibrium clusters when their motion freezes at low temperature. Helium provides unique advantages for the study of dislocations: Crystals are free of all but isotopic impurities, the concentration of these can be reduced to the parts per 10^9 (ppb) level, and the impurities are mobile at all temperatures and therefore remain in equilibrium with the dislocations. We have achieved a comprehensive study of the mechanical response of ^{4}He crystals to a driving strain as a function of temperature, frequency, and strain amplitude. The quality of our fits to the complete set of data strongly supports our assumption of stringlike vibrating dislocations. It leads to a precise determination of the distribution of dislocation network lengths and to detailed information about the interaction between dislocations and both thermal phonons and ^{3}He impurities. The width of the dissipation peak associated with impurity binding is larger than predicted by a simple Debye model, and much of this broadening is due to the distribution of network lengths.

DOI: 10.1103/PhysRevB.89.014105 PACS number(s): 67.80.B−, 61.72.Hh, 62.20.−x

I. INTRODUCTION

We have taken advantage of the unique properties of ^{4}He crystals to determine the distribution of lengths between nodes in their dislocation network and to study in detail the interaction between dislocations and both impurities and thermal phonons. We measured the shear modulus μ and the dissipation Q^{-1} associated with dislocation motion since such measurements provide detailed information about crystal defects [1,2]. The interaction between dislocations and impurity atoms is responsible for part of the dissipation but its microscopic mechanism is often controversial in usual materials [2,3]. Early models [4,5] proposed that the Cottrell atmosphere of impurities, which immobilizes dislocations at low temperature, can be dragged at high temperatures. The resulting dissipation produces a relaxation peak in Q^{-1} that is often broader than expected for a Debye process with a single relaxation time, but it is difficult to distinguish between the possible mechanisms for this broadening, e.g., impurity-impurity interactions [6] or a distribution of activation energies due to varying dislocation character [7]. The Q^{-1} peak width is also increased by variations in dislocation lengths, but the relevant network length distribution is very difficult to determine quantitatively in usual crystals. Transmission electron microscopy (TEM) [8] and etch pit images [9] provide some statistical information about dislocation networks and have been correlated with creep deformation. However, additional dislocations can be introduced when thin sections are prepared for TEM studies [10] and etch pit measurements only probe the dislocation network at the surface, which may be different from that of the bulk crystal. Recently, nondestructive measurements of dislocation numbers have been reported for microcrystals [11], but these were limited to small numbers of dislocations.

In hcp ^{4}He crystals, we have shown that dislocations move over large distances and produce exceptionally large changes in the elastic shear modulus μ and dissipation Q^{-1}. Furthermore, the dissipation due to impurity binding is not obscured by an overlapping dissipation peak due to kink-pair formation, in contrast to measurements in, e.g., hydrogenated nickel [12]. In ^{4}He crystals, we detected no effects of the lattice potential down to 20 mK [13]. In addition, the dissipation peak associated with impurities can be clearly distinguished from the dissipation from collisions with thermal phonons [14]. The only impurity is ^{3}He, whose concentration can be lowered far below 1 ppm [15]. As a consequence, elastic measurements in ^{4}He crystals are extremely sensitive probes of interactions between dislocations and either highly diluted impurities or thermal phonons. Ultimately, the behavior of dislocations in ^{4}He is of fundamental interest because of quantum effects which could be responsible for the absence of a Peierls barrier to dislocation motion, allowing them to glide freely. Dislocation cores may even be superfluid, which would allow "superclimb" [16] in addition to glide.

In this paper, we present the distribution $N(L_N)$ of lengths L_N between dislocation network nodes in a ^{4}He crystal and a comprehensive and quantitative explanation for the effects of phonon and impurity damping on the vibrations of its dislocations.

II. EXPERIMENT

We grew single crystals from ^{4}He with a ^{3}He concentration $x_3 = 0.3$ ppm inside a 5 cm^3 cell, which was made from a hexagonal hole in a 15 mm thick copper plate closed by two sapphire windows. The orientation of the crystal was determined from facets that appeared during growth at 600 mK [17] (Fig. 1). In this work, we chose a crystal with its sixfold axis of symmetry close to z, with spherical coordinates $\theta = 9.6^\circ$ and $\phi = 4.7^\circ$, where θ is the polar coordinate measured relative to z and ϕ is the azimuthal coordinate measured relative to x (Fig. 1). After establishing the orientation of the crystal, we regrew it from the superfluid liquid at 1.4 K so that any small liquid regions in the cell were solidified during

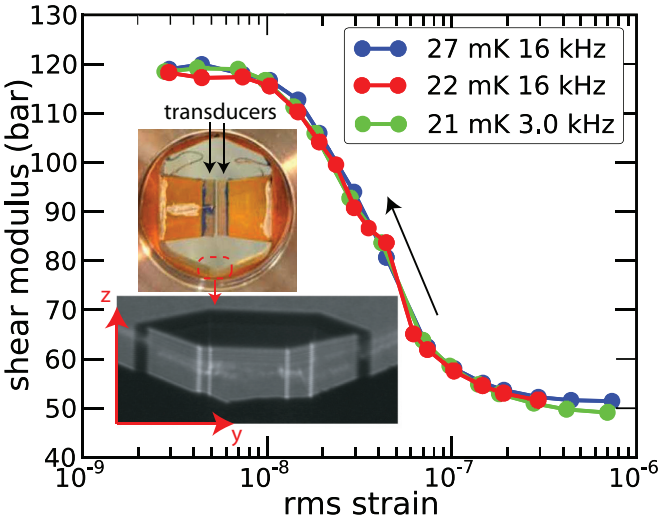

FIG. 1. (Color) Three recordings of the shear modulus measured while decreasing the driving strain near 25 mK. By analyzing the shape of the transition toward the intrinsic shear modulus $\mu_{\rm elastic}$ at low strain, we have determined the width of the distribution of network lengths. Insets: The experimental cell and the crystal as it grew from a seed at the bottom of the cell. The transducer plates lie in planes perpendicular to y and the motion of the left (drive) transducer is along z.

subsequent cooling. The temperature of the crystal was then maintained below 1 K so that it remained completely solid for all of the elastic measurements. This was important because small liquid regions would have trapped ^{3}He impurities at low temperature, leading to temperature variations of the total amount of ^{3}He in the crystal [15].

Inside the cell, two piezoelectric shear plates face each other with a separation $D = 0.7$ mm, forming a narrow gap that is filled with the oriented ^{4}He crystal (Fig. 1). Applying a voltage V to one transducer produces a shear strain $\epsilon = Vd_{15}/D$ in the ^{4}He in the gap, where $d_{15} = 0.95$ Å/V at the temperatures of our measurements [13]. The resulting stress in the ^{4}He in the gap is $\sigma = \mu\epsilon$, where μ is the shear modulus. This stress acts on the opposite transducer and generates a charge $d_{15}A\sigma$, which is detected as a current $i\omega d_{15}A\sigma = i\omega d_{15}^2\mu VA/D$, where $A = (1\ \text{cm})^2$ is the area of the transducers and ω is the drive frequency. This current was measured using a current preamplifier connected to a lock-in amplifier. In order to determine the dissipation Q^{-1} in the ^{4}He, which is the phase difference between σ and ϵ, we subtracted the additional phase shift due to the measurement electronics from the phase shift between V and the output of the lock-in.

The piezoelectric transducers were mounted so that the grounded sides were facing each other to minimize crosstalk, but there was a residual background signal due to a capacitive coupling inside the cell, probably between the wires soldered to the drive and detect transducers. With liquid ^{4}He in the cell at a pressure just below the melting curve, this capacitance was 1.03×10^{-14} F. This is close to the mechanical coupling due to the shear modulus of the crystal $d_{15}^2\mu_{\rm el}A/D = 1.6 \times 10^{-14}$ F, where $\mu_{\rm el} = 123$ bars is the maximum shear modulus for the crystal orientation in the present work. We carefully measured the pressure dependence of the capacitive background with the cell filled with liquid ^{4}He and found that it obeys the Clausius-Mosotti equation [18]. Since the change in the dielectric constant due to the change in density between the liquid and solid phases at the melting curve is negligible (less than 1%), we subtracted the background measured with liquid just below the melting pressure $P_{\rm m} = 25.3$ bars from the results of elastic measurements of the crystal.

III. THEORY

A. Dislocation glide

Dislocations glide in response to stress, allowing the crystal to slip on the glide plane [19]. This slip results in a strain $\epsilon_{\rm dis}$ that adds to the elastic strain $\epsilon_{\rm el}$ that would be present in the absence of dislocations, effectively reducing the shear modulus of the crystal. In hcp ^{4}He, dislocation glide only reduces the elastic coefficient c_{44} [13]. We chose the orientation of the crystal in the present work so that μ, the component of the elastic tensor that we measured, was very nearly equal to c_{44} (Appendix A). In the absence of mobile dislocations and at our working pressure $P_{\rm m}$, μ takes the value $\mu_{\rm el} = 123$ bars [20]. The effective shear modulus $\mu = \sigma/(\epsilon_{\rm dis} + \epsilon_{\rm el})$ is then given by

$$\mu = \frac{\mu_{\rm el}}{1 + \epsilon_{\rm dis}/\epsilon_{\rm el}}, \tag{1}$$

where $\mu_{\rm el} = \sigma/\epsilon_{\rm el}$. The dissipation is $Q^{-1} = \text{Im}[\mu]/\text{Re}[\mu]$.

In contrast to Zhou *et al.* [21,22], who assumed a large Peierls barrier against dislocation motion and made predictions that are inconsistent with experimental data [23], we model the dislocations as elastic strings [24] that bow out between pinning points in response to stress over our entire range of temperatures and driving strain. This model implies the equation of motion [24]

$$A\ddot{\xi} + B\dot{\xi} - C\frac{\partial^2\xi}{\partial x^2} = b\sigma, \tag{2}$$

where $\xi(x,t)$ is the dislocation displacement as a function of time t and position x between its pinning points, $A = \pi\rho b^2$ is the dislocation's effective mass per unit length in a material with density ρ, the term in B is the damping force per unit length, the term in C is the effective tension per length in a bowed-out dislocation, and $b\sigma$ is the effective force per length acting on the dislocation. [Because of our choice of crystal orientation, σ is very nearly equal to the resolved stress σ_4 (Appendix A).] For an edge dislocation,

$$C = [\mu_{\rm el}b^2/4\pi(1-\nu)][\ln(R/r)], \tag{3}$$

where ν is Poisson's ratio of the material in an isotropic approximation, R is the distance from the dislocation beyond which its stress field is canceled by neighboring dislocations (approximately the distance between dislocations), and r is the dislocation core radius [25]. In the present work, $\nu = 0.3$, $\rho = 191$ kg/m^3, $b = 3.7$ Å, $R \approx 100$ μm, $r \approx 1$ nm, $A = 8.2 \times 10^{-17}$ kg/m, and $C = 2.2 \times 10^{-12}$ N.

The resonant frequency of a dislocation of length L between pinning points is $\omega_0 = \pi\sqrt{C/A}/L$. It will be shown below that almost all of the dislocations in our crystal have $L < 300$ μm. Since $\omega_0(L = 300\ \mu\text{m})/2\pi \approx 300$ kHz, the drive frequency

ω in the present work is always much less than ω_0, so that the solution of Eq. (2) reduces to

$$\frac{\xi_0}{\sigma} = \frac{16bL^2}{\pi^5 C}\frac{1-i\omega\tau}{1+(\omega\tau)^2}, \tag{4}$$

where ξ_0 is the average oscillation amplitude along the length of the dislocation and we defined a relaxation time

$$\tau = BL^2/\pi^2 C. \tag{5}$$

The slip of the crystal due to glide of a dislocation is b times the fraction $\xi_0 L/A_g$ of the glide plane that has slipped, where A_g is the area of the glide plane. The corresponding contribution of the dislocation to the strain is $\xi_0 Lb/V$, where V is the volume of the crystal. We let $n(L)dL$ be the number of dislocations per unit volume with pinning length in a differential range around L so that the total contribution of all the dislocations to the strain is

$$\epsilon_{\rm dis} = \frac{b}{2}\int_0^\infty \xi_0(L)Ln(L)dL, \tag{6}$$

where the factor of 2 comes from averaging over the three possible $\langle 11\bar{2}0\rangle$ orientations of the Burgers vector in the basal plane of our hcp crystal. Substituting Eqs. (4) and (3) in Eq. (6) and using $\mu_{\rm el} = \sigma/\epsilon_{\rm el}$ yields

$$\frac{\epsilon_{\rm dis}}{\epsilon_{\rm el}} = \alpha\int_0^\infty L^3\frac{1-i\omega\tau}{1+(\omega\tau)^2}n(L)dL, \tag{7}$$

where $\alpha = 32(1-\nu)/\pi^4\ln(R/r)$. We emphasize that L is a generic dislocation pinning length and does not refer to a particular pinning mechanism. We also note that, in the present work, the elastic wavelength is greater than 1 cm, so that σ and ϵ are nearly uniform in the 0.7 mm gap between the transducers.

B. Impurity pinning

Dislocations in ^{4}He can be weakly pinned by bound ^{3}He impurities or strongly pinned by network nodes. We refer to a dislocation segment between network nodes as a network link with length L_N. Impurity binding occurs because the stress field surrounding a dislocation can lower the elastic energy associated with an impurity. The concentration of impurities near a dislocation is modified from the bulk concentration by a factor $\exp[-E_B/T]$, where E_B is the binding energy [26]. In solid ^{4}He, ^{3}He impurities are only weakly bound to dislocations, and it is possible to break a network link away from bound ^{3}He atoms at high stress.

If one starts at a high oscillating stress amplitude σ so that the network links are free of bound ^{3}He, the distribution of network lengths can be inferred from the shear modulus measured while decreasing σ. This argument is analogous to the one made by Iwasa in the context of torsional oscillator experiments [27]. As σ is decreased, binding of a ^{3}He atom to a network link is stable when σ reaches a critical value σ_c. At this point, the bound ^{3}He atom and the neighboring network nodes balance the force $\sigma_c bL_N$ applied to the network link, and the dislocation does not break away from the ^{3}He atom. The critical force $F_c = \sigma_c bL_N/2$ is the corresponding force on the ^{3}He atom and is determined by the shape of the binding potential. The bound ^{3}He atom divides the network link into two shorter segments that, by the same reasoning, can also be pinned by a ^{3}He atom at σ_c. ^{3}He atoms are available to do so because they are mobile even at zero temperature [28]. Thus the number of ^{3}He atoms pinning the dislocation suddenly increases to the thermal equilibrium value. The impurity-pinned network link no longer glides very much in response to σ, so μ increases. If there is a distribution of network lengths, the increase in μ due to impurity pinning occurs over a range in σ.

In order to obtain an expression for the distribution of network lengths $N(L_N)$, we consider the case of very low temperatures $T \ll E_B$. We first simplify Eq. (7). Since ^{3}He is the only impurity in our ^{4}He crystals, the critical force for breaking a network link away from a single impurity is always the same, and we can define a critical length $L_c = 2F_c/b\sigma$, which is the length of the network links that become pinned when the decreasing stress reaches σ. At $T \ll E_B$, the network links with $L_N < L_c$ are fully pinned by ^{3}He and do not contribute to $\epsilon_{\rm dis}/\epsilon_{\rm el}$ at all. Thus we can replace the lower limit of integration in Eq. (7) with $L_c(\epsilon)$, which we write as a function of $\epsilon = \sigma/\mu$ because ϵ is the quantity we directly control. The network lengths with $L_N > L_c$ have a length distribution given by $N(L_N)$, which is independent of σ because the network nodes are strong pinning sites. Thus we can also set $L = L_N$ and $n(L) = N(L_N)$ in Eq. (7), yielding

$$\frac{\epsilon_{\rm dis}}{\epsilon_{\rm el}} = \alpha\int_{L_c(\epsilon)}^\infty L_N^3\frac{1-i\omega\tau}{1+(\omega\tau)^2}N(L_N)dL_N. \tag{8}$$

The network links with $L_N > L_c$ are free of bound ^{3}He atoms, and measurements at different ^{3}He concentrations [13] demonstrate that the 300 parts per 10^9 (ppb) concentration of unbound ^{3}He in the present work is too small to significantly limit $\epsilon_{\rm dis}/\epsilon_{\rm el}$. Damping by thermal phonons is also negligible in the low temperature limit. Thus we must set $\tau = 0$ in Eq. (8):

$$\frac{\epsilon_{\rm dis}}{\epsilon_{\rm el}} = \alpha\int_{L_c(\epsilon)}^\infty L_N^3 N(L_N)dL_N. \tag{9}$$

From Eqs. (9) and (1) we obtain

$$N(L_c) = \frac{1}{\alpha L_c^3}\left(\frac{\mu}{\mu_{\rm el}}\right)^{-2}\frac{d}{dL_c}\left(\frac{\mu}{\mu_{\rm el}}\right). \tag{10}$$

The distribution of network lengths $N(L_N)$ is obtained from $N(L_c)$ by renaming the argument.

IV. RESULTS

A. Strain dependence at low T and high ω

We measured μ while decreasing ϵ to determine the form of $N(L_N)$. In order to prepare for the measurement of μ shown in Fig. 1, we started at 1 K where the crystal is soft because this is above the ^{3}He binding energy $E_B \approx 0.67$ K (Sec. IV D). Thus the dislocations were only pinned at network nodes and vibrated with large amplitudes [Eq. (4)]. We then cooled the crystal to a temperature near 25 mK under a high strain $\epsilon = 6.8\times10^{-7}$ at $\omega/2\pi > 3$ kHz. The crystal remained soft because the high strain prevented ^{3}He atoms from binding to the dislocations, even though the final temperature was well below E_B. Holding then the temperature constant, we decreased the applied strain in steps and measured

the equilibrium μ after waiting 1000 s at each step. We repeated this measurement at the indicated temperatures and frequencies (Fig. 1 legend), starting at 1 K each time, and $\mu(\epsilon)$ was reproduced to a high degree of accuracy.

The shear modulus gradually increased because ^{3}He impurities progressively bound to the dislocations as ϵ was decreased. If all the dislocations in our crystal had shared the same network length L_N, then μ in Fig. 1 would have jumped to μ_{el} when ϵ reached a critical strain, as explained in Sec. III B. The fact that the transition toward μ_{el} is spread over a rather large range in ϵ demonstrates that there is a broad distribution of L_N. Figure 1 also shows that increasing the temperature from 21 to 27 mK did not cause the stiffness of the crystal to decrease. The concentration of ^{3}He bound to dislocations must have decreased upon increasing the temperature, but the concentration was still high enough at $T = 27$ mK so that the impurity-pinned dislocations could not move. Thus the measurements of Fig. 1 were made in the low temperature limit assumed in Sec. III B and Eq. (10) can be used to determine $N(L_N)$. To do so we need to convert $\mu(\epsilon)$ (Fig. 1) to $\mu(L_c)$. This is possible if we know F_c since $\epsilon = 2F_c/bL_c\mu$. As explained below, we determined F_c from $\mu(T)$ and $Q^{-1}(T)$ in the phonon damping regime.

B. Temperature dependence at high ω and ϵ

Figure 2 shows μ and Q^{-1} measured while cooling from 1 K at $\omega/2\pi = 16$ kHz. The strain $\epsilon = 6.8 \times 10^{-7}$ was chosen to be high enough so that no ^{3}He atoms could bind to the dislocations as the temperature decreased. Thus the distribution of pinning lengths $n(L)$ remained equal to the distribution of network lengths $N(L_N)$, and only thermal phonons could damp the motion of the dislocations. The observed decrease in μ and Q^{-1} on cooling occurred because the number of thermal phonons decreased. After making the substitutions $L = L_N$, $n(L) = N(L_N)$, and $\tau = \tau_{ph}$ in Eq. (7),

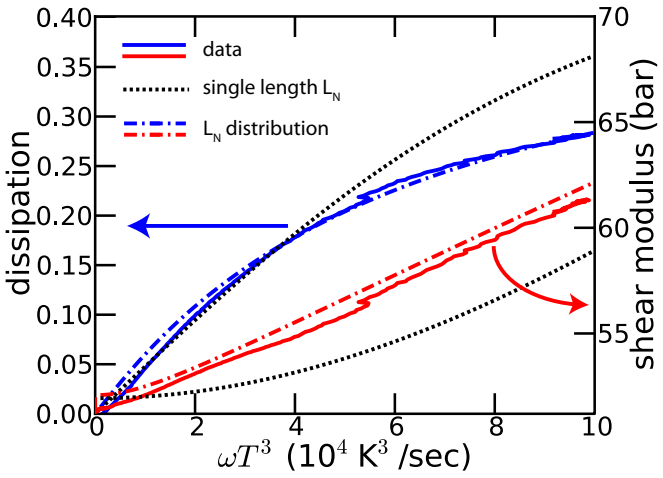

FIG. 2. (Color online) Solid curves: The shear modulus μ and the dissipation Q^{-1} measured while cooling from 1 K with an rms strain $\epsilon = 6.8 \times 10^{-7}$ at 16 kHz. Dotted curves: Calculations using a single network length as in our previous work [14], with best fit values $L_{N_0} = 96\ \mu$m and $\Lambda = 7.9 \times 10^5$ cm^{-2}. Dashed-dotted curves: Calculations using the length distribution from Eq. (10) and Fig. 1 after adjusting the critical force F_c to 6.8×10^{-15} N.

we obtain

$$\frac{\epsilon_{dis}}{\epsilon_{el}} = \alpha \int_0^\infty L_N^3 \frac{1 - i\omega\tau_{ph}}{1 + (\omega\tau_{ph})^2} N(L_N) dL_N, \qquad (11)$$

with $\tau_{ph} = B_{ph}L_N^2/\pi^2 C$ from Eq. (5). In the low temperature limit, damping occurs because incident phonons cause the dislocations to "flutter" and radiate elastic waves [29], yielding $B_{ph} = 14.4k_B^3T^3/\pi^2\hbar^2c^3$, where c is the Debye sound speed [30,31]. This is the reason why we plotted μ and Q^{-1} against $\omega T^3 \propto \omega\tau_{ph}$ in Fig. 2. The T dependence of μ and Q^{-1} can be calculated by substituting Eq. (11) into Eq. (1). Since $N(L_N)$ could only be determined from the data in Fig. 1 up to the value of F_c, we take F_c as a fitting parameter. The dashed-dotted curves in Fig. 2 show the calculated $\mu(T)$ and $Q^{-1}(T)$ for the best fit value $F_c = 6.8 \times 10^{-15}$ N. We obtain excellent agreement with our measurements over the entire range in T, which supports the form of $N(L_N)$ determined from the data in Fig. 1.

Haziot *et al.* [14] had fitted $\mu(T)$ and $Q^{-1}(T)$ in the phonon damping regime assuming a single length L_{N_0}. In this case $N(L_N) = N_{tot}\delta(L_N - L_{N_0})$, where N_{tot} is the total number of dislocations per unit volume and $\delta(x)$ is the Dirac delta function. Substituting this expression for $N(L_N)$ into Eq. (11) yields

$$\frac{\epsilon_{dis}}{\epsilon_{el}} = \alpha\Lambda L_{N_0}^2 \frac{1 - i\omega\tau_{ph}}{1 + (\omega\tau_{ph})^2}, \qquad (12)$$

where $\Lambda = N_{tot}L_{N_0}$ is the total dislocation length per unit volume. The black dotted curves in Fig. 2 show $\mu(T)$ and $Q^{-1}(T)$ calculated using Eq. (12) with the values $L_{N_0} = 96\ \mu$m and $\Lambda = 7.9 \times 10^5$ cm^{-2} chosen to optimize the agreement with the data in the low temperature limit. These black dotted curves depart from the data at high temperatures. This is further proof that a broad distribution in network length is necessary to understand the mechanical properties of ^{4}He crystals.

C. Network length distribution

Having determined F_c, we have now determined $N(L_N)$. The blue points in Fig. 3 show the shear modulus data at 27 mK and $\omega/2\pi = 16$ kHz from Fig. 1, now plotted as a function of $L_c = 2F_c/b\epsilon\mu$. The red curve is $N(L_N)$ obtained from the blue points using Eq. (10). We have only plotted $N(L_N)$ over the range $20\ \mu\text{m} < L_N < 300\ \mu$m corresponding to dislocations that contribute significantly to the softening, i.e., the range in L_c over which μ is varying (Fig. 3 blue points). Although there may be a large number of dislocations with $L_N < 20\mu$m, they do not contribute measurably because of the L_N^3 dependence of $\epsilon_{dis}/\epsilon_{el}$ [Eq. (9)]. At the opposite extreme, there are very few dislocations with $L_N > 300\ \mu$m. Extending the range of integration beyond $20\ \mu\text{m} < L_N < 300\ \mu$m in any of the calculations in the present work does not affect the results. As expected, the single network length $L_{N_0} = 96\mu$m obtained from the simplified model of Ref. [14] is near the middle of this range.

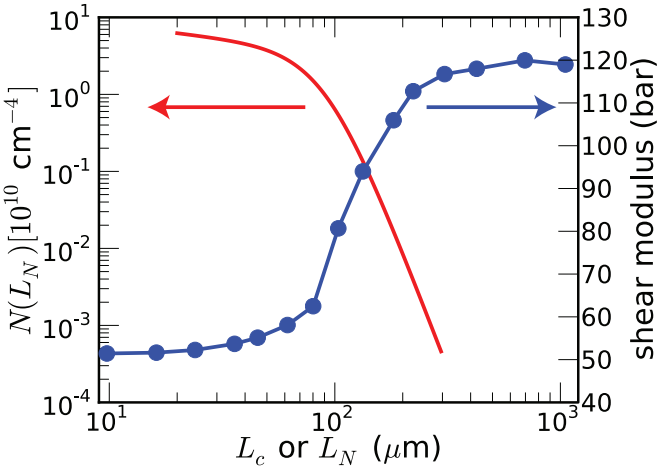

FIG. 3. (Color) Blue points: The shear modulus at 27 mK and 16 kHz from Fig. 1 as a function of the critical length $L_c = 2F_c/b\mu\epsilon$ (see text). Red curve: The distribution $N(L_N)$ over the range of lengths that contribute significantly to the softening, derived from the blue points using Eq. (10).

D. Temperature dependence at low ω and ϵ

Given these results, it is now possible to analyze the effect of damping by bound ^{3}He impurities. The data in Fig. 1 were acquired in the low temperature limit, so that dislocations with bound ^{3}He atoms did not contribute to $\epsilon_{\mathrm{dis}}/\epsilon_{\mathrm{el}}$. Now we present a temperature dependent measurement and study the transition due to thermal binding of ^{3}He to the dislocations. Figure 4 shows $\mu(T)$ and $Q^{-1}(T)$ measured on cooling at low frequencies and low strain $\epsilon = 5.4 \times 10^{-9}$. At high temperatures, at least up to 1 K, the crystal is soft with a temperature independent μ, indicating that damping of dislocation motion by thermal phonons is negligible at these drive frequencies. The high temperature value of μ in Fig. 4 is the same as the low temperature value of μ in Fig. 2 since in both cases the dislocations vibrate freely between network nodes. The difference in the temperatures at which the dislocation motion is unaffected by both thermal phonons and ^{3}He comes from the difference in the drive amplitude and frequencies. At low temperatures in Fig. 4, μ reaches the intrinsic value μ_{el}. The behavior of $\mu(T)$ and $Q^{-1}(T)$ at intermediate temperatures is frequency dependent: At each frequency $\omega/2\pi$, we observed a Q^{-1} peak at a temperature $T_{\mathrm{p}}(\omega)$ nearly coincident with the midpoint of the transition in μ, and $T_{\mathrm{p}}(\omega)$ increases with ω.

We expect $\epsilon_{\mathrm{dis}}/\epsilon_{\mathrm{el}}$ in these measurements to be given by Eq. (7). In this equation, binding of ^{3}He to dislocations can change $\epsilon_{\mathrm{dis}}/\epsilon_{\mathrm{el}}$ by changing $n(L)$ or τ. The frequency dependence of T_{p} suggests that changes in τ dominate in the measurements of Fig. 4. Figure 5 shows $\log\omega$ plotted against $1/T_{\mathrm{p}}(\omega)$ for the measurements shown in Fig. 4 as well as additional measurements of this type on the same crystal but at different ϵ and ω. The measurements at $\epsilon = 2.7 \times 10^{-9}$ show a transition between frequency dependent T_{p} at small ω and frequency independent T_{p} at large ω. The measurements at $\epsilon = 1.1 \times 10^{-8}$ show the same transition, but at a smaller ω. The transition, in fact, occurs at a critical dislocation speed [32]. Below the critical speed, changes in $\epsilon_{\mathrm{dis}}/\epsilon_{\mathrm{el}}$ result from changes in τ, while above the critical speed, changes in $\epsilon_{\mathrm{dis}}/\epsilon_{\mathrm{el}}$ result from changes in $n(L)$. This implies that below the critical speed ^{3}He atoms move with the dislocations and damp their motion, while above the critical speed they approximate static pinning sites. Figure 5 shows that the measurements in Fig. 4 were made well below the critical dislocation speed. Thus, for these measurements, the distribution of pinning lengths remains equal to the distribution of network lengths as the crystal is cooled from 1 K. Making the substitutions $L = L_N$, $n(L) = N(L_N)$, and $\tau = \tau_3$ in Eq. (7) yields

$$\frac{\epsilon_{\mathrm{dis}}}{\epsilon_{\mathrm{el}}} = \alpha \int_0^\infty L_N^3 \frac{1 - i\omega\tau_3}{1 + (\omega\tau_3)^2} N(L_N) dL_N, \qquad (13)$$

where $\tau_3 = B_3 L_N^2/\pi^2 C$ from Eq. (5). We assume, as in previous work [33], that the ^{3}He damping force is proportional to the concentration of ^{3}He bound to the dislocations, so that the damping constant has the form $B_3 = B_3^\infty \exp[E_B/T]$.

We can estimate the binding energy E_B by considering the case of a single network length L_{N_0}. As in the derivation

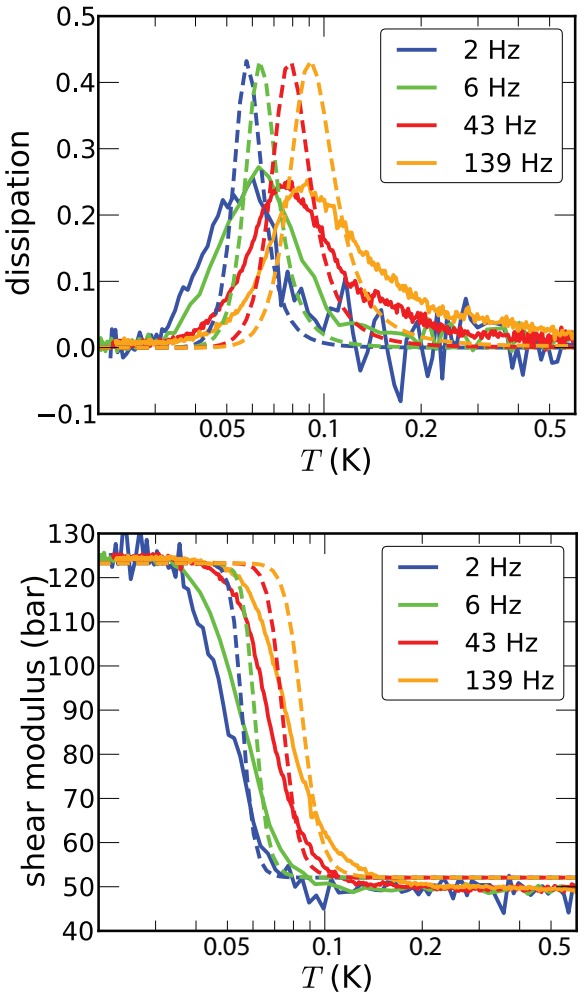

FIG. 4. (Color) The dissipation (a) and the shear modulus (b) measured while cooling from 1 K at low strain 5.4×10^{-9}. Dashed curves: Calculations using a single network length $L_{N_0} = 96$ μm, a dislocation density $\Lambda = 7.9 \times 10^5$ cm^{-2}, and a single binding energy $E_B = 0.67$ K.

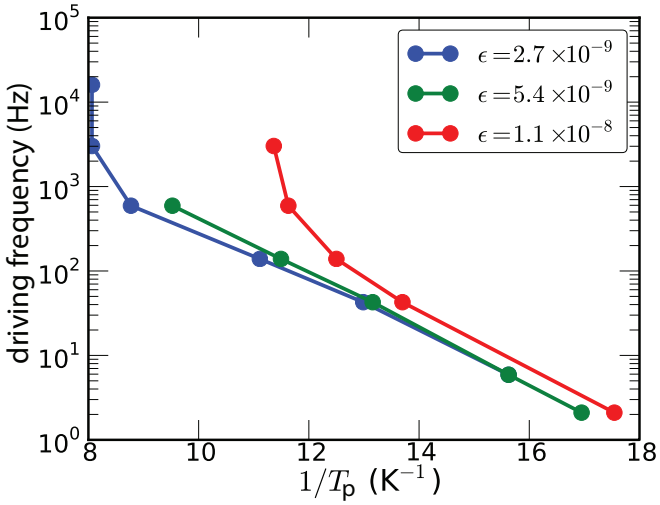

FIG. 5. (Color) Arrhenius plot of the driving frequency vs the inverse temperature of the Q^{-1} peak at low strain ϵ. This shows the transition from ^{3}He damping at low dislocation speeds to ^{3}He pinning at high dislocation speeds [32].

of Eq. (12), we substitute $N(L_N) = N_{\rm tot}\delta(L_N - L_{N_0})$ into Eq. (13) to obtain

$$\frac{\epsilon_{\rm dis}}{\epsilon_{\rm el}} = \alpha \Lambda L_{N_0}^2 \frac{1 - i\omega\tau_3}{1 + (\omega\tau_3)^2}. \tag{14}$$

It is shown in Appendix B that Eq. (14) implies the following Arrhenius equation relating T_p and ω:

$$\ln \omega = \ln\left(\frac{\sqrt{1+s}}{\tau_0}\right) - E_B/T_p, \tag{15}$$

where $s = \alpha \Lambda L_{N_0}^2$ and $\tau_0 = B_3^\infty L_N^2/\pi^2 C$. We fitted Eq. (15) to the low frequency, linear part of the data obtained at $\epsilon = 2.7 \times 10^{-9}$ in Fig. 5 in order to obtain the initial estimates $E_B = 0.67$ K and $B_3^\infty = 2.6 \times 10^{-9}$ N s/m^2 for use in the subsequent calculations.

In Fig. 4, we show $\mu(T)$ and $Q^{-1}(T)$ calculated using Eqs. (14) and (1) with a single network length $L_{N_0} = 96$ μm and dislocation density $\Lambda = 7.9 \times 10^5$ cm^{-2} (from Fig. 2), a single binding energy $E_B = 0.67$ K, and a damping coefficient $B_3^\infty = 2.6 \times 10^{-9}$ N s/m^2. In Fig. 6, we show $\mu(T)$ and $Q^{-1}(T)$ calculated using Eqs. (13) and (1) with $N(L_N)$ from Fig. 3 and the same values of E_B and B_3^∞. The calculated and measured Q^{-1} peak temperatures $T_{\rm p}(\omega)$ are in good agreement in both Figs. 4 and 6. The overall agreement between theory and data is better in Fig. 6 than in Fig. 4, but it is not perfect in Fig. 6: The magnitude and temperature width of the Q^{-1} peak were respectively 140% and 64% of the measured values. In order to obtain an excellent fit, we had to account for the distribution in binding energies that was first proposed in Ref. [34].

One expects such a distribution because E_B depends on the screw and edge character of the dislocations [35], and variations in the dislocation character were observed in x-ray images of subboundaries of ^{4}He crystals [36]. The large softening that we observed, which implies large ΛL_N^2, requires the existence of such subboundaries [14]. Thus we add a

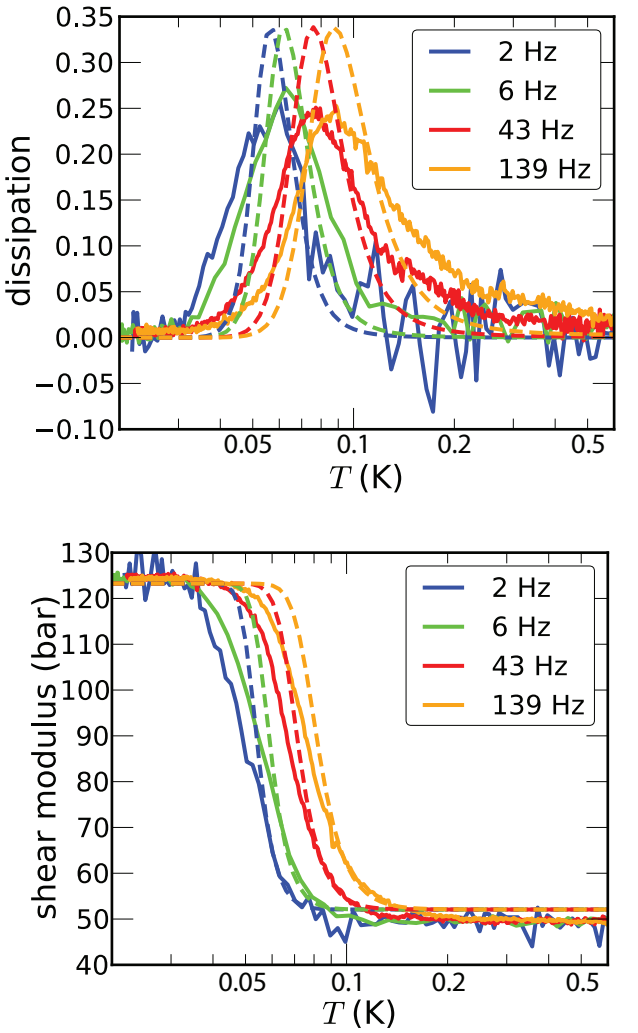

FIG. 6. (Color) Same data as in Fig. 4 compared with a calculation (dashed curves) using the length distribution of Fig. 3 and a single binding energy $E_B = 0.67$ K.

distribution of binding energies $p(E_B)$ to Eq. (13):

$$\frac{\epsilon_{\rm dis}}{\epsilon_{\rm el}} = \alpha \int_0^\infty L_N^3 \int_0^\infty \frac{1 - i\omega\tau_3}{1 + (\omega\tau_3)^2} p(E_B) N(L_N) dE_B dL_N.$$

The distribution $p(E_B)$ must have an upper cutoff. In order to effectively satisfy this constraint and to facilitate comparison with earlier work [34], we choose a log-normal form,

$$p(E_B) = \frac{\exp[-(\ln E_B - m)^2/s^2]}{\sqrt{\pi} s E_B}, \tag{16}$$

with mean $\langle E_B \rangle = \exp[m + s^2/4]$ and variance $\langle E_B \rangle^2[\exp(s^2/2) - 1]$. We obtain an excellent fit to the data with $\langle E_B \rangle = 0.67$ K and a standard deviation of 0.1 K (dashed curves Fig. 7). As expected, $\langle E_B \rangle$ is the same as the binding energy determined in Ref. [32], where the distribution of E_B was not considered. Our best fit value of $\langle E_B \rangle$ also shows that our determination of F_c (Fig. 2) is reasonable, since F_c is the maximum magnitude of the spatial derivative of E_B where the ^{3}He atom is bound and it has a numerical value $\approx \langle E_B \rangle / 4b$. The quality of the fits in Fig. 7 is better

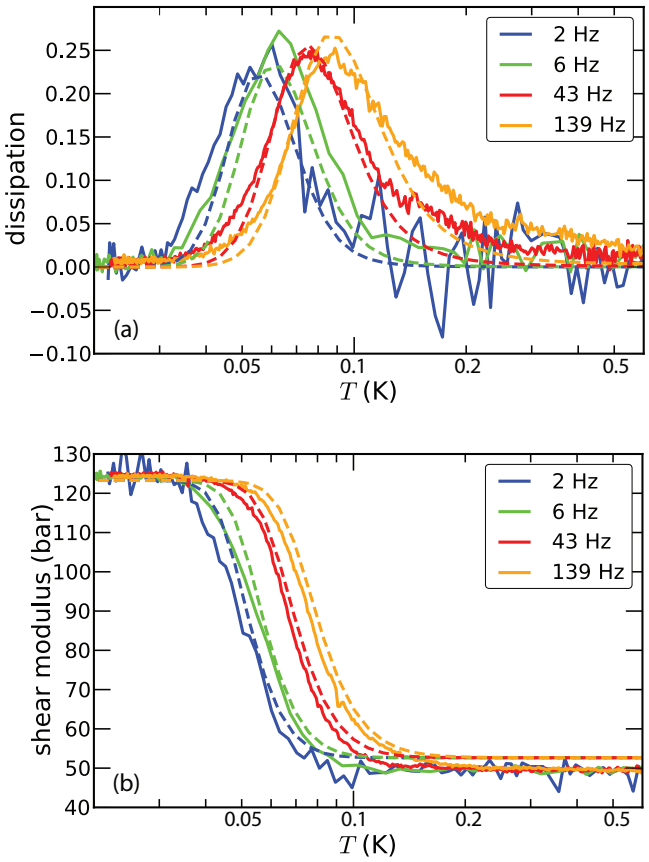

FIG. 7. (Color) Same data as in Fig. 4 compared with a calculation (dashed curves) using the length distribution of Fig. 3 and a log-normal distribution of binding energies E_B with mean 0.67 K and standard deviation 0.1 K.

than that of the fits to $\mu(T)$ and $Q^{-1}(T)$ in Ref. [37]. In that work, unlike the present work, the frequency dependence was not studied and the fits in the ^{3}He binding regime were not constrained by fits to measurements of phonon damping.

V. DISCUSSION AND CONCLUSION

As discussed in Ref. [32], there is a critical dislocation speed below which ^{3}He atoms move with the dislocations and damp their motion. Above the critical speed, ^{3}He atoms approximate static pinning sites. We established above that the measurements in Fig. 7 were made below the critical dislocation speed. Some previous frequency dependent measurements of $\mu(T)$ and $Q^{-1}(T)$ in ^{4}He polycrystals were interpreted in terms of a Debye model with a distribution of activation energies [34]. The equations that yielded the best fits to $\mu(T)$ and $Q^{-1}(T)$ in that work are equivalent to the ones used to calculate $\mu(T)$ and $Q^{-1}(T)$ in Fig. 7 in the limit of small softening ΛL_N^2 and a single dislocation network length. The standard deviation of the distribution of binding energies that was determined in Ref. [34] is 2.5 times larger than in the present work, perhaps because the distribution of network lengths was not considered in Ref. [34].

The resonant period of a torsional oscillator containing solid helium decreases with the shear modulus of the helium [38]. Many if not all of the torsional oscillator results initially explained by supersolidity of ^{4}He can be explained by this effect [39,40]. In Ref. [27], results of torsional oscillator experiments were explained in terms of ^{3}He pinning of dislocations. This explanation could be consistent with the model used in the present work if the dislocations were moving faster than the critical dislocation speed in the torsional oscillator measurements that were analyzed. To verify this, it would be necessary to study the frequency dependence of a torsional oscillator measurement at constant response amplitude, analogously to Fig. 5. In Ref. [27], the distribution of network lengths was determined, up to the critical force, from the dependence of the period shift on the rim speed in the torsional oscillator experiment of Ref. [41]. Thus the method for determining the form of the network length distribution was analogous to the one used in the present work. However, it was apparently impossible to observe phonon damping in the torsional oscillator measurements analyzed in Ref. [27], and the critical force was left as a free parameter in the fit to the temperature dependence of the period shift, unlike the fit to the temperature dependence of μ and Q^{-1} in Fig. 7 of the present work. After optimizing the value of the critical force, the best fit period shift as a function of temperature was a factor of 1.45 below the measured period shift in Ref. [27].

In conclusion, we used the unique properties of helium crystals to measure the length distribution of a dislocation network. We showed that it was necessary to account for this broad distribution to obtain a complete, consistent, and quantitative interpretation of the mechanical properties of these crystals as a function of temperature, amplitude, and frequency of driving strain in both the phonon and ^{3}He damping regimes. In so doing, we obtained detailed information about the interactions between the dislocations and ^{3}He impurities. We hope that this work inspires calculations of the ^{3}He binding energy as a function of the screw and edge character of the dislocation to which the ^{3}He atom is bound.

ACKNOWLEDGMENT

This work was supported by Grant No. ERC-AdG 247258 SUPERSOLID, and by a grant from NSERC Canada.

APPENDIX A: CRYSTAL ORIENTATION DEPENDENCE

For clarity of presentation in the equations of the main text, we neglected the small angle between our crystal's sixfold axis of symmetry and the z direction defined in Fig. 1, but we accounted for this small angle in our calculations. The elastic coefficients of a hcp crystal can be labeled using Voigt notation, where the subscripts 1,2,3,4,5,6 correspond to the coordinates $x'x', y'y', z'z', y'z', x'z', x'y'$ in a Cartesian coordinate system where z' is aligned with the sixfold axis of symmetry (the elastic coefficients are invariant under rotations about z'). In hcp ^{4}He, c_{44} is the only elastic coefficient that is reduced by dislocation glide [13], so that $\epsilon_4 = (\epsilon_{\rm dis} + \epsilon_{\rm el})$. Since $c_{44} = \sigma_4/\epsilon_4$, we can replace Eq. (1) by

$$c_{44} = \frac{c_{44}^{\rm el}}{1 + \epsilon_{\rm dis}/\epsilon_{\rm el}}, \tag{A1}$$

where $\epsilon_{el} = \sigma_4/c_{44}^{el}$ and $c_{44}^{el} = 124$ bars is the value of c_{44} in the absence of mobile dislocations at our working pressure of 25.3 bars [20]. The stress σ must be replaced by σ_4 in Eqs. (2) and (4), but we note that Eq. (7) remains the same due to cancellation of the factor σ_4. In order to obtain the theoretical curves in the figures of the main text, we substituted Eq. (A1) into

$$\mu = 0.97c_{44} + 0.03c_{66}^{el}, \tag{A2}$$

where $c_{66}^{el} = 96.0$ bars. Equation (A2) follows from the orientation our crystal (Sec. II) and the general expression for μ given in the supplement to Ref. [13] for arbitrary crystal orientation.

To fit the measurement of $\mu(\epsilon)$ shown in blue in Fig. 3, we substituted the fitting function

$$\frac{c_{44}}{c_{44}^{el}} = \frac{\tanh\left[c_1(\ln L_c + c_0)\right]}{c_2} + c_3 \tag{A3}$$

into Eq. (A2) and obtained best fit values $c_0 = 9.05$, $c_1 = 1.83$, $c_2 = 3.36$, and $c_3 = 0.703$.

APPENDIX B: ARRHENIUS EQUATION

Substituting Eq. (14) into Eq. (1) yields

$$\frac{\mu}{\mu_{el}} = \frac{1 + s + (\omega\tau_3)^2 + i\omega\tau_3 s}{(1+s)^2 + (\omega\tau_3)^2}, \tag{B1}$$

where $s \equiv \alpha\Lambda L_{N_0}^2$ and $\tau_3 = B_3 L_N^2/\pi^2 C$. Since $Q^{-1} = \mathrm{Im}[\mu]/\mathrm{Re}[\mu]$, we have

$$Q^{-1} = \frac{\omega\tau_3 s}{1 + s + (\omega\tau_3)^2}. \tag{B2}$$

The dissipation attains a maximum value $Q_{max}^{-1} = s/2\sqrt{1+s}$ for $\omega\tau_3 = \sqrt{1+s}$. We defined the temperature at which Q^{-1} is maximized as T_p in the main text. Thus

$$\omega\tau_0 \exp[E/T_p] = \sqrt{1+s}, \tag{B3}$$

where $\tau_0 = B_3^{\infty} L_N^2/\pi^2 C$. Rearranging Eq. (B3) yields Eq. (15).

[1] A. S. Nowick and B. S. Berry, *Anelastic Relaxation in Crystalline Solids* (Academic, New York, 1972).
[2] M. S. Blanter, I. S. Golovin, H. Neuhauser, and H.-R. Sinning, *Internal Friction in Metallic Materials* (Springer, Berlin, 2007), Chap. 2.
[3] I. Ritchie, Scr. Metall. Mater. **16**, 249 (1982).
[4] J. Friedel, C. Boulanger, and C. Crussard, Acta Metall. Mater. **3**, 380 (1955).
[5] G. Schoeck, Acta Metall. Mater. **11**, 617 (1963).
[6] L. Magalas, J. Phys. IV **6**, C8–163 (1996).
[7] H. Numakura, Y. Minonishi, and M. Koiwa, Philos. Mag. A **63**, 785 (1991).
[8] J. Bilde-Sörensen, Acta Metall. Mater. **21**, 1495 (1973).
[9] P. Lin, S. Lee, and A. Ardell, Acta Metall. Mater. **37**, 739 (1989).
[10] R. Tsui, Acta Metall. Mater. **15**, 1723 (1967).
[11] V. L. R. Jacques, D. Carbone, R. Ghisleni, and L. Thilly, Phys. Rev. Lett. **111**, 065503 (2013).
[12] K. Tanaka, T. Inukai, K. Uchida, and M. Yamada, J. Appl. Phys. **54**, 6890 (1983).
[13] A. Haziot, X. Rojas, A. D. Fefferman, J. R. Beamish, and S. Balibar, Phys. Rev. Lett. **110**, 035301 (2013).
[14] A. Haziot, A. D. Fefferman, J. R. Beamish, and S. Balibar, Phys. Rev. B **87**, 060509 (2013).
[15] C. Pantalei, X. Rojas, D. Edwards, H. Maris, and S. Balibar, J. Low Temp. Phys. **159**, 452 (2010).
[16] S. G. Söyler, A. B. Kuklov, L. Pollet, N. V. Prokof'ev, and B. V. Svistunov, Phys. Rev. Lett. **103**, 175301 (2009).
[17] S. Balibar, H. Alles, and A. Y. Parshin, Rev. Mod. Phys. **77**, 317 (2005).
[18] M. Chan, M. Ryschkewitsch, and H. Meyer, J. Low Temp. Phys. **26**, 211 (1977).
[19] D. Hull and D. Bacon, *Introduction to Dislocations* (Butterworth-Heinemann Elsevier, Oxford, UK, 2000), Chap. 3.
[20] D. S. Greywall, Phys. Rev. B **16**, 5127 (1977).
[21] C. Zhou, J.-J. Su, M. J. Graf, C. Reichhardt, A. V. Balatsky, and I. J. Beyerlein, Philos. Mag. Lett. **92**, 608 (2012).
[22] C. Zhou, J.-J. Su, M. J. Graf, C. Reichhardt, A. V. Balatsky, and I. J. Beyerlein, Phys. Rev. B **88**, 024513 (2013).
[23] A. Haziot, X. Rojas, A. D. Fefferman, J. R. Beamish, and S. Balibar, Phys. Rev. Lett. **111**, 119602 (2013).
[24] A. Granato and K. Lucke, J. Appl. Phys. **27**, 583 (1956).
[25] J. P. Hirth and J. Lothe, *Theory of Dislocations*, 2nd (ed.) (Krieger, Malabar, FL, 1964), Eq. (3-52).
[26] D. Hull and D. Bacon, *Introduction to Dislocations* (Ref. [19]), Chap. 10.
[27] I. Iwasa, J. Low Temp. Phys. **171**, 30 (2013).
[28] A. R. Allen, M. G. Richards, and J. Schratter, J. Low Temp. Phys. **47**, 289 (1982).
[29] J. M. Ziman, *Electrons and Phonons* (Oxford University Press, Oxford, UK, 2001), Chap. 6.
[30] T. Ninomiya, J. Phys. Soc. Jpn **36**, 399 (1974).
[31] T. Ninomiya, Scr. Metall. Mater. **18**, 669 (1984).
[32] A. Haziot, A. D. Fefferman, F. Souris, J. R. Beamish, H. J. Maris, and S. Balibar, Phys. Rev. B **88**, 014106 (2013).
[33] I. Iwasa, Phys. Rev. B **81**, 104527 (2010).
[34] O. Syshchenko, J. Day, and J. Beamish, Phys. Rev. Lett. **104**, 195301 (2010).
[35] D. Hull and D. Bacon, *Introduction to Dislocations* (Ref. [19]), Chap. 4.
[36] I. Iwasa, H. Suzuki, T. Suzuki, T. Nakajima, H. Yonenaga, H. Suzuki, H. Koizumi, Y. Nishio, and J. Ota, J. Low Temp. Phys. **100**, 147 (1987).
[37] E. S. H. Kang, H. Yoon, and E. Kim, arXiv:1211.5593.
[38] H. Maris and S. Balibar, J. Low Temp. Phys. **162**, 12 (2011).
[39] H. J. Maris, Phys. Rev. B **86**, 020502 (2012).
[40] J. R. Beamish, A. D. Fefferman, A. Haziot, X. Rojas, and S. Balibar, Phys. Rev. B **85**, 180501 (2012).
[41] Y. Aoki, J. C. Graves, and H. Kojima, Phys. Rev. Lett. **99**, 015301 (2007).